Transactions on Computer Science and Intelligent Systems Research
ISSN: 2960-1800, eISSN: 2960-2238 | Volume 7
TPCEE 2024

Research on heliostat field optimization model based on particle swarm optimization

Feiyang Ding[1], Rongjing Wang[1,*], Jiazheng Song[1], Yuxin Qian[2], Xiaohan Yang[1]

[1]School of Zhang Jian, Nantong University, Nantong, China, 226019

[2]School of Mathematics and Statistics, Nantong University, Nantong, China, 226019

* Corresponding Author Email: 2479003080wrj@gmail.com

Abstract. In the face of the global demand for carbon reduction, the construction of new energy power system has become the key. The traditional power system is facing the pressure of transformation, and the innovative application of new energy technology is imminent. This paper establishes an optimal design model for a heliostat mirror field, aiming at the efficient use of solar energy and the improvement of heat collection efficiency and performance. The model reduces power generation cost and enhances market competitiveness by optimising the layout and tracking strategy. The research results not only promote the development of solar thermal power generation technology, but also provide a reference for other new energy projects, which is of great significance to achieve the goal of carbon peak and carbon neutrality.

Keywords: Euler Rotation Matrix; Particle Swarm Algorithm; Shadow Occlusion Efficiency.

1. Introduction

The construction of a new energy-dominated power system is a key measure to achieve China's carbon peak and carbon neutrality goals. Tower-type solar thermal power generation is a low-carbon, environmentally friendly clean energy technology. The core component of the tower-type solar thermal power station is the heliostat, whose base includes a longitudinal shaft and a horizontal shaft. The planar reflector is mounted on the horizontal shaft, and the longitudinal shaft controls the azimuth angle of the reflector, while the horizontal shaft controls the pitch angle of the reflector. The intersection point of the two shafts, which is the center point of the heliostat, is called the installation height above ground. Tower-type power stations rely on a large number of heliostats to form a heliostat field, which reflects sunlight onto a collector, where the collector heats a thermal medium and stores solar energy in the form of heat energy, which is then converted into electrical energy through heat exchange. The incident light of sunlight has a certain cone angle [1], so the reflected light is also conical. During operation, the control system adjusts the normal direction of the heliostat in real time according to the position of the sun to ensure that the reflected light is accurately directed towards the center of the collector, which is called the absorption tower height.

When studying the shadow occlusion efficiency model, simplified models such as numerical simulation models [2]and distributed parameter models [3] are commonly used. Numerical simulation models use computer simulation technology to establish a virtual model of the heliostat field and simulate the propagation and reflection process of solar radiation in the field. By adjusting model parameters, the changes in shadow occlusion under different conditions can be observed. Distributed parameter models divide the heliostat field into multiple small regions, and the shadow occlusion conditions within each element can be calculated independently. By considering the interactions between elements such as radiation spillover and occlusion, the shadow occlusion efficiency of the entire field can be obtained. However, these models fail to fully consider the impact of absorption towers on heliostats, resulting in certain deviations in the model. These models ignore the shadow and occlusion effects that absorption towers may have on heliostats. In order to improve the computational efficiency of the model, this article uses particle swarm optimization and further optimizes it by introducing dynamic inertia weight and combining with Euler rotation matrix for

single-objective optimization, reducing the number of iterations and shortening the running time, significantly improving the efficiency of the heliostat field, achieving an average annual output thermal power of 32.8105 MW and an average output thermal power per unit mirror area of 0.5223 MW / m^2.

2. The basic funamental of heliostat field optimization design

2.1. Modeling Shadow Occlusion Efficiency

When part of the mirror of a heliostat is in the shadow of other neighboring heliostats and cannot receive the sun's rays is called shading, as shown in the left panel of Figure 1. When a portion of the reflected light from a fixed-sun mirror cannot reach the heat absorber because the backs of other neighboring fixed-sun mirrors are blocking the light, it is called shading, as shown in the right panel of Figure 1. The shadowing blocking efficiency is the ratio of the effective area of the mirror surface of the heliostat that is not affected by shadowing and blocking to the total area of the mirror surface of the heliostat.

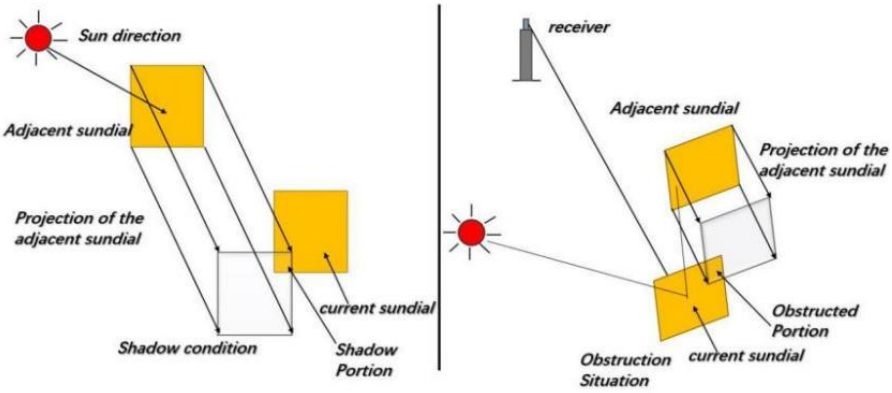

Figure 1. Shadow occlusion situation

2.1.1. Geometric Projection

The geometric projection method is used to determine whether the target heliostat will be occluded by determining whether other heliostats will cast shadows on the target heliostat. According to Figure 2(a) and Figure 2(b), a top view and a side view of the shadow judgment rectangle can be obtained. From these two views, two sets of side lengths of the rectangle for shadow judgment can be obtained, denoted as $L1$ and $L2$, respectively.

$$\begin{cases} L_1 = 2L_m \\ L_2 = \omega_m / \sin\Phi_c \end{cases} \tag{1}$$

where, L_m and ω_m are the length and width of the sizer, respectively.

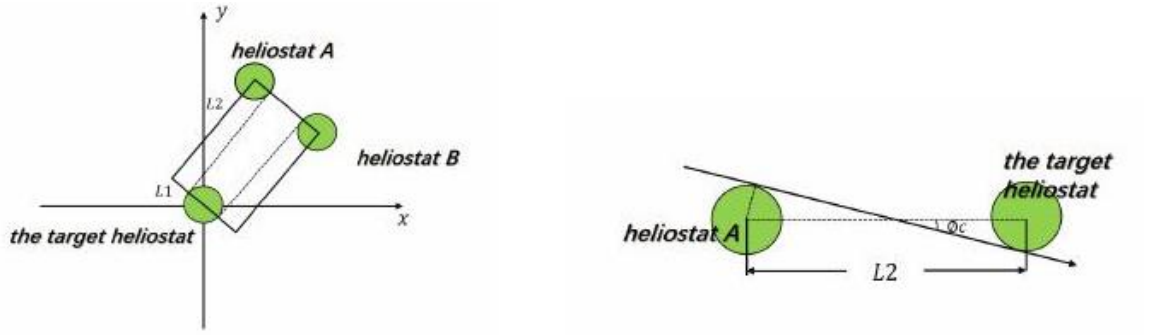

(a)Determining the top view of a rectangl (b)Determining the side view of a rectangle

Figure 2. Determining the different views of a rectangle

Further find the coordinates of the four vertices $P1 \sqcup P4$ of the judgment rectangle [4], which can be obtained by the following method:

$$\begin{cases} P1:\begin{cases} x_{p1}=x_h+L_1 \cdot u_y \\ y_{p1}=y_h+L_1 \cdot u_x \end{cases} \\ P2:\begin{cases} x_{p2}=x_h+L_1 \cdot u_y \\ y_{p2}=y_h-L_1 \cdot u_x \end{cases} \\ P3:\begin{cases} x_{p3}=x_h+L_1 \cdot u_y+L2 \cdot u_x \\ y_{p3}=y_h-L_1 \cdot u_x+L2 \cdot u_y \end{cases} \\ P4:\begin{cases} x_{p4}=x_h-L_1 \cdot u_y+L2 \cdot u_x \\ y_{p4}=y_h+L_1 \cdot u_x+L2 \cdot u_y \end{cases} \end{cases} \tag{2}$$

where, $(\mathrm{x_h}, y_h, z_h)$ is the coordinates of the mirror center of the target heliostat, the u_x and u_y expressions are as follows:

$$\begin{cases} u_x=\dfrac{x_h}{\sqrt{{x_h}^2+{y_h}^2}} \\ u_y=\dfrac{y_h}{\sqrt{{x_h}^2+{y_h}^2}} \end{cases} \tag{3}$$

Based on the shadow judgment rectangle and other information about the position of the heliostat, it is determined whether the heliostat may be shadowing the target heliostat. By considering reflected light, it is also possible to identify fixers that may be shading the target fixer.

2.1.2. Coordinate transformation of random points on a specular surface

In geometric projection, random points are placed in the heliostat coordinate system to ensure that they are within the mirror [5]. For ray tracing work, an Eulerian rotation matrix method is used to transform these points from the heliostat coordinate system to the ground coordinate system.

The spatial Cartesian coordinate system XYZ is rotated by β angles about the Z -axis to form a new coordinate system:

$$(x'_A, y'_A, z'_A)=R_z(\beta)(x_A, y_{A,} z_A)^T \tag{4}$$

where, $R_Z(\beta)$ is the Euler rotation matrix:

$$R_Z(\beta)=\begin{bmatrix} \cos\beta & -\sin\beta & 0 \\ \sin\beta & \cos\beta & 0 \\ 0 & 0 & 1 \end{bmatrix} \tag{5}$$

In a similar way:

$$R_x(\varphi)=\begin{bmatrix} 1 & 0 & 0 \\ 0 & \cos\varphi & -\sin\varphi \\ 0 & \sin\varphi & \cos\varphi \end{bmatrix}, R_\gamma(\gamma)=\begin{bmatrix} \cos\gamma & 0 & \sin\gamma \\ 0 & 1 & 0 \\ -\sin\gamma & 0 & \cos\gamma \end{bmatrix} \tag{6}$$

Where, φ, γ are the angles of rotation of the coordinate system XYZ about the X -axis and Y -axis respectively.

When the coordinates of a random mirror point are converted from a heliograph coordinate system to a terrestrial coordinate system, the axis of rotation and the angle of rotation are determined first, and then the conversion is performed.

$$(x'_A, y'_A, z'_A)=R_z(\beta)\cdot R_y(\gamma)\cdot R_x(\phi)\cdot(x_A, y_A, z_A)^T \tag{7}$$

The ground region formed by the coordinate transformation of the points simulated with the Eulerian rotation matrix method is occluded by the projections of the neighboring heliographs on the ground, as shown in Figure 3:

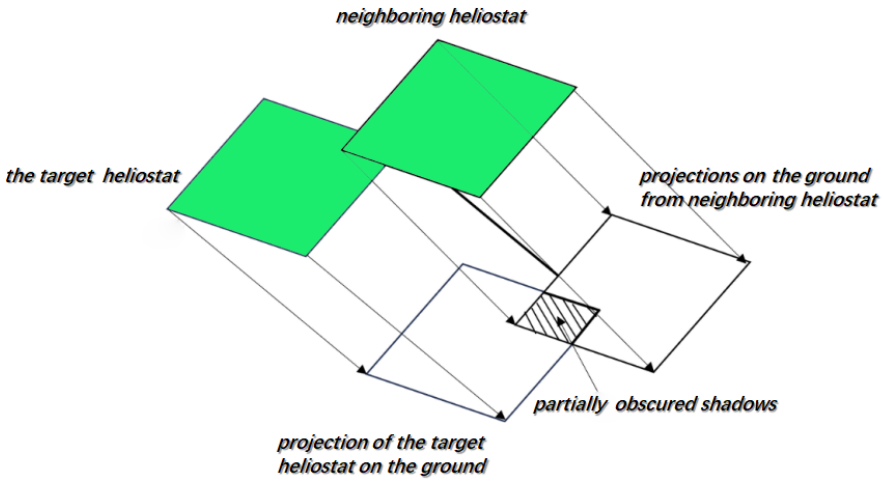

Figure 3. Occlusion judgement matrix

2.1.3. A method for determining whether a random point on a target mirror is occluded by a shadow

Judgement by shadows:

In the shadow determination phase, the four vertices of the heliostat are projected onto the ground to form a parallelogram using the two-dimensional judgment rule. Then, determining whether a random point of light is inside the heliostat is the same as determining whether the point is inside the parallelogram.

Two-dimensional judgment rule for the shaded stage: According to Figure 4, if point E is inside a parallelogram, then $AE = uAD + vAB$, then the decision coefficients satisfy $u \geq 0$, $v \leq 1$. Result: the expression of the judgment coefficient u, v is as follows:

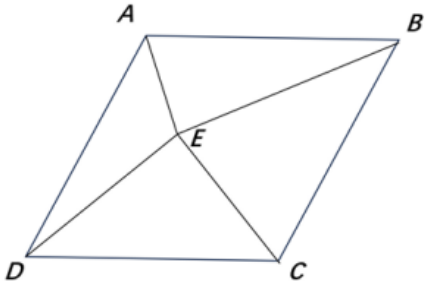

Figure 4. Parallelogram judgement diagram

$$\begin{cases} u=\dfrac{aa\cdot bc-ab\cdot ac}{aa\cdot bb-ab\cdot ab} \\ v=\dfrac{bb\cdot ac-bc\cdot ab}{aa\cdot bb-ab\cdot ab} \end{cases} \begin{cases} ax = x_B - x_A \\ ay = y_B - y_A \\ bx = x_D - x_A \\ by = y_D - y_A \\ cx = x_E - x_A \\ cy = y_E - y_A \end{cases} \begin{cases} aa = ax\cdot ax + ay\cdot ay \\ ab = ax\cdot bx + ay\cdot by \\ ac = ax\cdot cx + ay\cdot cy \\ bb = bx\cdot bx + by\cdot by \\ bc = bx\cdot cx + by\cdot cy \end{cases} \tag{8}$$

By comparing shading to determine the center coordinates of rectangles and other heliostats, it is possible to determine which heliostat may cause shading to block the target heliostat. In the case of reflected light, an occlusion judgment rectangle is used to determine which heliostat may be blocking the target heliostat.

Occlusion determination:

During the masking phase, a two-dimensional judgment rule is used to determine the intersection of the reflected light with the surrounding fixed-sun mirrors. Determining the coordinates of the projection of the reflected light from the ground relative to the vertices of each heliostat transforms the problem into determining whether the intersections of the reflected light with the other heliostats are within a rectangular heliostat in three-dimensional space. The determination is made by checking whether the angles formed by the points of the rectangle and the four vertices are acute.

$$\begin{cases} \cos EAD = (x_E - x_A)\cdot(x_D - x_A) + (y_E - y_A)\cdot(y_D - y_A) + (z_E - z_A)\cdot(z_D - z_A) \\ \cos EDC = (x_E - x_D)\cdot(x_C - x_D) + (y_E - y_D)\cdot(y_C - y_D) + (z_E - z_D)\cdot(z_C - z_D) \\ \cos ECB = (x_E - x_C)\cdot(x_B - x_C) + (y_E - y_C)\cdot(y_B - y_C) + (z_E - z_C)\cdot(z_B - z_C) \\ \cos EBA = (x_E - x_B)\cdot(x_A - x_B) + (y_E - y_B)\cdot(y_A - y_B) + (z_E - z_B)\cdot(z_A - z_B) \end{cases} \tag{9}$$

The resulting shadow efficiency:

$$\eta_{sb} = 1 - Shadow\ Occlusion\ Loss = 1 - \frac{N_{sb}}{N} \tag{10}$$

where, N_{sb} is the number of blocked photons, N is the total photon count.

2.2. Modeling of annual average thermal power output per unit mirror area

The optical efficiency of the heliostat [6]is:

$$\eta = \eta_{sb}\eta_{\cos}\eta_{at}\eta_{trunc}\eta_{ref} \tag{11}$$

where, the values of η_{at} [7], $\eta_{\cos}$ [8], η_{trunc} [9]are known by reference, and the values of η_{sb} is determined by equations (10), respectively. η_{ref} is the mirror reflectance, which can be set to a constant, e.g. 0.92.

The output thermal power of the heliostat field is:

$$E_{field} = DNI \cdot \sum_{i=1}^{N} A_i\eta_i \tag{12}$$

where, DNI is the normal direct radiation irradiance, N is the total number of heliostats (in units of faces), A_i is the light area of the ith fixation mirror (unit: m^2), η_i is the optical efficiency of the ith mirror.

Then the average annual thermal power output per unit mirror area [10]is:

$$p = \frac{\sum_{j=1}^{12} \frac{E_{field}}{S}(j)}{12} = \frac{\sum_{j=1}^{12} \frac{DNI \cdot \sum_{i=1}^{N} A_i\eta_i}{\sum_{i}^{N} A_i}}{12} \tag{13}$$

where, S is the sum of the lighting areas of all the fixed-sun mirrors. $\frac{E_{(field)}}{S}(j)$ denotes the average thermal power output per unit of mirror in the jth month.

2.3. Particle swarm algorithm modeling

The particle swarm algorithm (PSO) [11-12] approximates the optimal solution step by step by simulating the search process of individuals (particles) in the solution space and utilizing the

information sharing among individuals. In the optimized design of heliostat field, PSO algorithm searches for the optimal configuration of the absorber tower coordinates, heliostat dimensions, mounting height and total number of particles by adjusting the particle velocity and position. The objective function is as follows:

$$\max\left(\frac{\text{average annual thermal power}}{\text{unit surface area of mirrors}}\right)-\lambda\cdot n\text{umber of heliostats} \tag{14}$$

where, λ is a weighting factor to balance effectiveness and cost.

Algorithmic Processes:

Initialization: Initialize the particle swarm, each particle represents a possible heliostat field configuration, including the absorber tower coordinates, heliostat dimensions, mounting height and total number. Initialize the velocity and position of the particles, the velocity represents the search direction and step size of the particles.

Adaptation evaluation: calculate the adaptation value of each particle, which is determined by the objective function. Specific calculations include the average annual thermal power, mirror area and number of heliostats for each particle.

Update individual optimum and global optimum: Compare the fitness value of each particle with its historical optimum fitness value, and update the individual optimum if the current value is better. Compare the individual optimal values of all particles to find the global optimal value.

Velocity and position update: Update the velocity and position of each particle according to the formula:

$$\begin{aligned} v_i^{t+1} &= \omega v_i^t + c_1 r_1 (p_i^{best} - x_i^t) + c_2 r_2 (g^{best} - x_i^t) \\ x_i^{t+1} &= x_i^t + v_i^{t+1} \end{aligned} \tag{15}$$

where, v_i^t denotes the velocity of particle i at the tth iteration, x_i^t denoting the position of particle i at the tth iteration, ω is inertia weight. $c1$ and $c2$ are the acceleration constants, $r1$ and $r2$ are random numbers, p_i^{best} is the all-time best position for particle i, g^{best} is the best position in the game.

3. Results

3.1. Results and analyses corresponding to the shadowing occlusion efficiency model

By constructing an optimisation model of shadow blocking efficiency and annual average output thermal power per unit mirror area, the performance of heliostat mirrors has been successfully improved, with the annual average optical efficiency reaching 0.5594 and shadow blocking efficiency as high as 0.8966, which in turn pushes the annual average output thermal power of the heliostat field up to 32.8105 and the annual average output thermal power per unit mirror area up to 0.5223. In order to demonstrate this result, a weighted heat map has been created to clearly present the efficient working status of each heliostat. In order to visualise this result, a weighted heat map has been produced, taking 9:00 on 21 st January as an example, which clearly presents the efficient working state of each heliostat mirror, highlighting the great potential of high-efficiency energy conversion technology.

Figure 5(a) illustrates a weighted heat map of the shadowing obscuration efficiency of heliostats, revealing contrasting regions of high and low efficiency, although the effect of mutual obscuration between heliostats is usually limited. Figure 5(b) An in-depth analysis of the optical performance of heliostats using an optical efficiency-weighted heat map shows significant regional variations in optical efficiency, which is a particular constraint on the overall efficiency of the system, highlighting its key role in system optimisation.

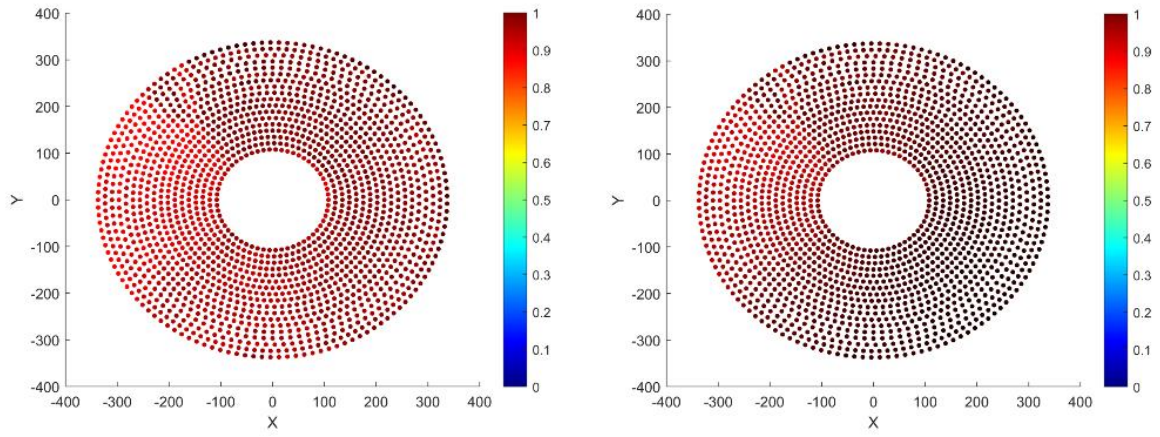

(a) Shadow Masking Efficiency Chart (b) Optical efficiency chart

Figure 5. Weighted heat map

A series of key outputs have been designed to fully evaluate and optimise the performance of the system for a given heliostat size, mounting height and heliostat centre position. These parameters cover the annual average optical efficiency derived from the solution, the annual average cosine efficiency, the annual average output thermal power, etc., and are further refined to the annual average output thermal power that can be contributed per unit mirror area. Table 1 details these key metrics and provides an important basis for quantitatively evaluating system performance.

Table 1. Average Optical Efficiency and Power Output on 21st day of each month

Date	Average optical efficiency	Average cosine efficiency	Average shadow shading efficiency	Average cut-off efficiency	Average thermal power output per unit area of mirror (kw / m^2)
21-January	0.541	0.741	0.869	0.932	0.480
21-February	0.609	0.761	0.972	0.920	0.598
21-March	0.627	0.780	1.000	0.901	0.646
21-April	0.627	0.790	1.000	0.889	0.655
21-May	0.627	0.792	1.000	0.887	0.657
21-June	0.627	0.789	1.000	0.891	0.654
21-July	0.628	0.778	1.000	0.903	0.644
21-August	0.600	0.759	0.958	0.921	0.582
21-September	0.530	0.737	0.852	0.933	0.458
21-October	0.4382	0.718	0.712	0.939	0.306
21-November	0.410	0.711	0.665	0.941	0.259
21-December	0.449	0.720	0.729	0.938	0.327

From the data, it can be seen that there are fluctuations in the average optical efficiency from month to month, which are related to seasonal changes, weather conditions and system maintenance. The average shading efficiency, average truncation efficiency and cosine efficiency also show some differences in different months, reflecting the performance of the heliostat system under different conditions. The shading efficiency is relatively stable throughout the year, which is related to the shading resistance considered in the system design.

By solving the shadowing masking efficiency model, the cosine efficiency model, the truncated efficiency model, and the output thermal power model obtain Table 2.

Table 2. Average optical efficiency and output power

Average annual optical efficiency	Average annual cosine efficiency	Average annual shadow shading efficiency	Average annual cut-off efficiency	Average annual thermal power output	Average thermal power output per unit area of mirror (kw/m^2)
0.560	0.756	0.897	0.916	32.810	0.522

3.2. Results and analyses corresponding to the particle swarm model

Based on the above model, the optimisation of the heliostat field needs to follow the "optimality criterion": maximise the average annual thermal power per mirror and minimise the number of heliostats to control the cost. The particle swarm algorithm was used to accurately solve for the coordinates of the absorber tower, the uniform sizes and mounting heights of the heliostats, and the optimal total number of mirrors. Under the condition of maintaining the rated annual average thermal power output of the heliostat field at 60 MW , it not only ensures high-efficiency output, but also reduces the cost by reasonably controlling the number of heliostats. By comprehensively considering the changes of the absorption tower location, heliostat size, installation height and location layout, the optimised annual average optical efficiency, annual average output thermal power and annual average output thermal power per unit mirror area were obtained, as shown in Table 3, which achieved the dual optimisation goals of efficiency and economy.

The average optical efficiency fluctuates significantly from month to month, which is affected by seasonal changes, weather variations, and system maintenance conditions. Meanwhile, the average shading efficiency, truncation efficiency and cosine efficiency also show monthly differences, which reflect the adaptability and performance of the heliostat system under different light and weather conditions. However, the shading efficiency remains relatively stable throughout the year, which demonstrates the careful consideration and enhancement of shading resistance during the design stage of the system.

Table 3. Average optical efficiency and output power on 21st of each month

Date	Average optical efficiency	Average cosine efficiency	Average shadow shading efficiency	Average cut-off efficiency	Average thermal power output per unit area of mirror (kw/m^2)
21-January	0.660	0.855	0.968	0.892	1.181
21-February	0.686	0.869	0.972	0.910	1.198
21-March	0.723	0.889	0.998	0.911	1.346
21-April	0.744	0.897	1.000	0.930	1.355
21-May	0.763	0.912	1.000	0.937	1.457
21-June	0.738	0.897	1.000	0.921	1.354
21-July	0.690	0.858	0.986	0.913	1.244
21-August	0.670	0.859	0.969	0.901	1.182
21-September	0.636	0.837	0.953	0.893	1.095
21-October	0.592	0.817	0.912	0.889	1.006
21-November	0.582	0.811	0.905	0.889	0.959
21-December	0.617	0.840	0.930	0.885	0.927

Table 4 is obtained by solving the shadow shading efficiency model, the cosine efficiency model, the truncated efficiency model, and the output thermal power model:

Table 4. Average optical efficiency and output power

Average annual optical efficiency	Average annual cosine efficiency	Average annual shadow shading efficiency	Average annual cut-off efficiency	Average annual thermal power output	Average thermal power output per unit area of mirror (kw / m^2)
0.675	0.862	0.966	0.906	60.128	1.192

Optical and cosine efficiencies are important measures of the system's light harvesting capability, while shading and truncation efficiencies reflect the system's ability to minimise energy loss. The annual average thermal power output per unit area of mirror data, on the other hand, directly correlates to the thermal conversion efficiency of the system and the energy yield in practical applications.

When maximising the annual average thermal power output per unit mirror area of the heliostat field, data on the positional coordinates of the absorber tower, heliostat dimensions, mounting height, number of heliostats, and total area of heliostats were obtained as shown in Table 5:

Table 5. Design parameters for heliostats

Absorption tower position coordinates	Heliostats Size (Width× Height)	Installation height of heliostats (m)	Total number of heliostats	Total area of heliostat (m^2)
(15.7,12.3)	5.35×4.2	5.83	1967	44198.49

4. Conclusions

In this paper, by constructing and optimising the design model, the heat collection efficiency and overall performance of a fixed-sun mirror field in a tower solar thermal power system are significantly improved. Aiming at the common challenge of shadow shading in fixed-sun mirror fields, this paper innovatively proposes an optimisation strategy combining the particle swarm algorithm and Eulerian rotation matrix. Using a numerical simulation model and a distributed parameter model, not only does the numerical simulation model quantify the shadowing effect in depth, but also comprehensively explores the specific influence of the absorber tower on the performance of the heliostat field, which reveals the limitations of the traditional model in this regard.

The results show that the optimisation method effectively makes up for the shortcomings of the traditional model in dealing with the influence of the absorption tower, and significantly improves the computational efficiency, reduces the number of iterations and significantly shortens the running time through the introduction of particle swarm algorithm. This breakthrough has achieved excellent results in the design and optimisation practice of the heliostat mirror field, which not only enhances the economy of tower solar thermal power generation and reduces the power generation cost, but also significantly improves its market competitiveness, and injects new vitality into the development of new energy power generation field.

References

[1] ZhangPing, XiZhengwen, Hua Wenhan, et al. Calculation method of optical efficiency of solar tower thermal mirror field[J]. Technology and Market, 2021, 28(6): 5-8.

[2] Yang Yikun, Xu Xinxin, Tian Wenpeng. Dual-motor synchronous coupling model based on numerical simulation[J]. Collection, 2018, 11.

[3] Chen Zhongyu, Xu Jin, Wang Keyou, et al. Generalized comprehensive load model considering follower and support distributed photovoltaics and two-stage parameter aggregation equivalent method[J]. Electric Power Automation Equipment Dianli Zidonghua Shebei, 2023, 43(3).

[4] Gao Weidong. Research on scheduling optimization of heliostat field in tower solar power station[D]. North China Electric Power University, 2021.

[5] Ding Qi, Zeng Zhiyong, Chen Wuzhong, et al. A method for evaluating the effective mirror area of a heliostat field[J]. Acta Energiae Solaris Sinica, 2021, 42(9): 184.

[6] Wang S, Asselineau C A, Fontalvo A, et al. Co-optimisation of the heliostat field and receiver for concentrated solar power plants[J]. Applied Energy, 2023, 348: 121513.

[7] Noone C J, Torrilhon M, Mitsos A. Heliostat field optimization: A new computationally efficient model and biomimetic layout[J]. Solar Energy, 2012, 86(2): 792-803.

[8] Zheng D, Lu Yinli, Hu Yudong, et al. Calculation model of output thermal power of heliostat mirror field[J]. Journal of Taizhou University,2024,46(03):1-8.

[9] Yang Hongtao. Research on heliostat concentrating model and optimal scheduling system[D]. Xi'an University of Technology,2023.

[10] Hussaini Z A, King P, Sansom C. Numerical simulation and design of multi-tower concentrated solar power fields[J]. Sustainability, 2020, 12(6): 2402.

[11] Liu Z, Wei Z, Li J. Optimization of Heliostat Field Arrangement Model Based on Geometric Relationship and Particle Swarm Algorithm[C]. IEEE 4th International Conference on Power, Electronics and Computer Applications (ICPECA), 2024: 365-373.

[12] Li Q, Li G, Wang X. Optimal Design Model of Heliostat Field[C]. IEEE International Conference on Electrical, Automation and Computer Engineering (ICEACE), 2023: 1260-1265.